

Theory of electron-plasmon coupling in semiconductors

Fabio Caruso and Feliciano Giustino

Department of Materials, University of Oxford, Parks Road, Oxford, OX1 3PH

(Dated: April 13, 2016)

The ability to manipulate plasmons is driving new developments in electronics, optics, sensing, energy, and medicine. Despite the massive momentum of experimental research in this direction, a predictive quantum-mechanical framework for describing electron-plasmon interactions in real materials is still missing. Here, starting from a many-body Green's function approach, we develop an *ab initio* approach for investigating electron-plasmon coupling in solids. As a first demonstration of this methodology, we show that electron-plasmon scattering is the primary mechanism for the cooling of hot carriers in doped silicon, it is key to explain measured electron mobilities at high doping, and it leads to a quantum zero-point renormalization of the band gap in agreement with experiment.

Plasmons are collective oscillations of electrons in solids that can exist even in the absence of an external driving field. During the last decade plasmons generated tremendous interest owing to the rise of plasmonics, the science of manipulating light and light-matter interactions using surface plasmon polaritons [1]. Plasmonic materials and devices show exceptional promise in the areas of nanoelectronics [2], photovoltaics [3, 4], and radiation treatment therapy [5, 6]. While the electrodynamic laws governing plasmonics at macroscopic length-scales are well understood [7, 8], little is known about the interaction of plasmons with matter at the atomic scale. For example questions pertaining the interaction between plasmons and charge carriers in semiconductors have not been addressed on quantitative grounds, yet they are critical to engineering materials for semiconductor plasmonics [9]. Up to now microscopic quantum-mechanical theories of electron-plasmon interactions have been limited to idealised models of solids, such as the homogeneous electron gas [10, 11]. While these models laid the theoretical foundations of the theory, they are not suitable for predictive calculations.

In this work we introduce a first-principles method to study electron-plasmon coupling in solids. As a first application we focus on doped semiconductors, where the manifestations of electron-plasmon coupling are most spectacular. In contrast to metals and insulators, doped semiconductors can sustain ‘thermal plasmons’, that is plasmons with energies comparable to those of lattice vibrations. Under these conditions electron-plasmon interactions can modify carrier lifetimes, mobilities, and optical gaps in a manner similar to electron-phonon interactions. Using this method we find that, in the case of degenerate *n*-type silicon, thermal plasmons lead to ultrafast relaxation of hot carriers, provide the main bottleneck to carrier mobility, and induce a zero-point renormalization of the band gap that exceeds the phonon-induced renormalization.

In free-electron metals the energy of a plasmon is $\hbar\omega_P = (\hbar^2 e^2 n / \epsilon_0 m_e)^{1/2}$, where \hbar is the Planck constant, ϵ_0 is the dielectric permittivity of vacuum, and e , m_e , and n

are the electron charge, mass, and density, respectively. At typical metallic densities, as in common plasmonic metals such as Au and Ag ($n = 3\text{--}8 \cdot 10^{22} \text{ cm}^{-3}$), plasmons have characteristic energies in the range of 5-10 eV. In these cases electron-plasmon scattering is suppressed by the energy-conservation selection rule. At variance with this scenario, in doped semiconductors the electron mass in the above expression is replaced by the band effective mass, and the vacuum permittivity is replaced by the dielectric constant. As a result the plasmon energy is considerably smaller, and at standard doping levels it can easily reach the thermal range, $\hbar\omega_P = 10\text{--}100 \text{ meV}$. Under these conditions electrons can exchange energy with plasmons, hence the populations of carriers and plasmons become mutually coupled.

In order to investigate the consequences of this coupling, we start by characterizing plasmonic excitations in doped silicon from first principles. Figure 1 shows the calculated electron energy loss function, $\text{Im } \epsilon^{-1}(\mathbf{q}, \omega)$, which encodes information about how an electron traveling through a solid dissipates energy [12]. Here $\epsilon^{-1}(\mathbf{q}, \omega)$ denotes the head of the inverse dielectric matrix for the wavevector \mathbf{q} and the frequency ω , evaluated within the random phase approximation [13, 14]. In the case of intrinsic silicon at zero temperature (Fig. 1a) the loss function exhibits a continuous energy distribution (brown region) with a threshold set by the fundamental gap. This broad structure arises from interband transitions from the filled valence bands to the empty conduction bands, and physically corresponds to the generation of electron-hole pairs by impact ionization. This is schematically indicated as ‘process 1’ in Fig. 1d. The scenario changes drastically in the case of doped silicon. Fig. 1b and Fig. 1c show the loss function of heavily *n*-doped silicon, corresponding to $n = 2.5 \cdot 10^{19} \text{ cm}^{-3}$ and $n = 2.5 \cdot 10^{20} \text{ cm}^{-3}$, respectively. As a result of the partial filling of the conduction band valley near the *X* point of the Brillouin zone, new dissipation channels become available. In particular, ‘process 2’ in Fig. 1b corresponds to the generation of low-energy electron-hole pairs. In this case we see sharp structures which define

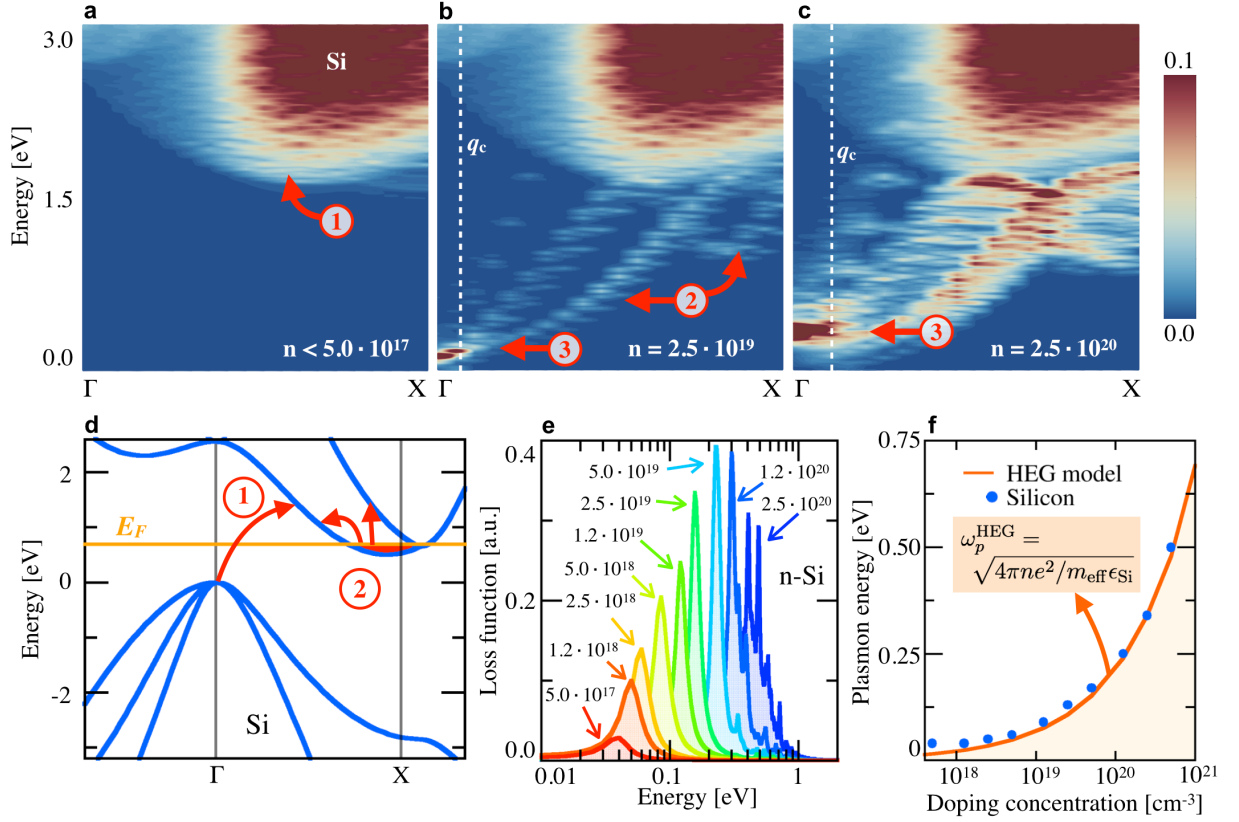


Figure 1. (a–c) Calculated electron-energy loss function of n -type silicon for momentum transfers \mathbf{q} along the Γ X high-symmetry line. The carrier density increases from left to right, from 10^{17} to 10^{20} cm^{-3} . (d) LDA band structure of silicon, and Fermi level (E_F) for $n = 2.5 \cdot 10^{20} \text{ cm}^{-3}$. The step-like structures in (b) and (c) are only a numerical artifact arising from the limited Brillouin-zone sampling. (e) Variation of the plasmon peak in the loss function vs. carrier density, evaluated at $\mathbf{q} = 0$. (f) Plasma energies extracted from peaks in (e), plotted vs. carrier concentration (blue dots). The red line corresponds to the analytical result obtained for a homogeneous electron gas with the calculated isotropic effective mass and dielectric constant of silicon ($m_{\text{eff}} = 0.25$, $\epsilon_{\text{Si}} = 12$).

‘ghost’ bands as a function of the momentum loss $\hbar\mathbf{q}$. These features are understood in terms of intraband and interband transitions from occupied initial states with wavevector \mathbf{k} near the bottom of the conduction band to empty final states of wavevector $\mathbf{k} + \mathbf{q}$. The intensity of these features increases with the doping level from Fig. 1b to Fig. 1c. The peaks in the loss function denoted by ‘process 3’ cannot be explained in terms of the previous two mechanisms. In fact for $\mathbf{q} = 0$ these structures are much sharper than those described above, and exist below the energy (momentum) threshold for the generation of electron-hole pairs via interband (intraband) transitions. These processes correspond to the emission of plasmons, and are characterised by well-defined energy resonances, as it is shown by Fig. 1e for $\mathbf{q} = 0$. By mapping these plasmon peaks in the loss function we can see in Fig. 1f that the plasmon energy $\hbar\omega_P$ scales with the carrier concentration, following the same trend expected for a homogeneous electron gas. In this figure we also see that the plasmon energy is highly tunable

via doping, from thermal energies at carrier densities around 10^{18} cm^{-3} , to half an electronvolt at densities near 10^{21} cm^{-3} .

At large momentum transfer $\hbar\mathbf{q}$ the distinction between plasmons and electron-hole pairs is no longer meaningful, since the fluctuations of the charge density happen on length-scales approaching the size of the crystal unit cell. In the following we identify plasmons in the loss function by analogy with the homogeneous electron gas, where well-defined plasma excitations exist only for momenta below the electron-hole continuum [15]. For a plasmon of energy $\hbar\omega_P$ the critical momentum is given by the wavevector $q_c = k_F [(1 + \hbar\omega_P/\epsilon_F)^{1/2} - 1]$, with k_F and ϵ_F being the Fermi wavevector and the Fermi energy, respectively. The critical wavevector q_c marks the onset of Landau damping, that is, the decay of a plasmon upon excitation of an electron-hole pair. Thus, for $q < q_c$ thermal plasmons are undamped collective phenomena with lifetimes set by plasmon-phonon and plasmon-plasmon scattering processes [16]. This boundary is shown as

white dashed lines in Fig. 1b and Fig. 1c.

In order to investigate the effects of plasmons on the electronic structure we generalise Pines' theory of electron-plasmon interactions in the homogeneous electron gas [15] to *ab initio* calculations for crystalline solids. Our strategy consists of the following steps: (i) We identify the energy vs. wavevector dispersion relations of thermal plasmons. This is achieved by determining the plasma energies from the poles of $\text{Im } \epsilon^{-1}(\mathbf{q}, \omega)$

for momenta below the critical wavevector q_c [20]. (ii) We single out the plasmonic contribution to the macroscopic dielectric function ϵ_M via the Taylor expansion $\epsilon_P(\mathbf{q} + \mathbf{G}, \omega) = \frac{\partial \epsilon_M}{\partial \omega} \big|_{\omega=\omega_P(\mathbf{q})} [\omega - \omega_P(\mathbf{q})] + i\eta$ in the vicinity of the plasmon frequency $\omega_P(\mathbf{q})$. (iii) We calculate the electron-plasmon self-energy starting from many-body perturbation theory, and retain only the plasmonic screening. This leads to the retarded electron self-energy in Raleigh-Schrödinger perturbation theory [21]:

$$\Sigma_{n\mathbf{k}}^{\text{eP}} = \int \frac{d\mathbf{q}}{\Omega_{\text{BZ}}} \sum_m |g_{mn}^{\text{eP}}(\mathbf{k}, \mathbf{q})|^2 \left[\frac{n_{\mathbf{q}} + f_{m\mathbf{k}+\mathbf{q}}}{\varepsilon_{n\mathbf{k}} - \varepsilon_{m\mathbf{k}+\mathbf{q}} + \hbar\omega_P(\mathbf{q}) + i\eta} + \frac{n_{\mathbf{q}} + 1 - f_{m\mathbf{k}+\mathbf{q}}}{\varepsilon_{n\mathbf{k}} - \varepsilon_{m\mathbf{k}+\mathbf{q}} - \hbar\omega_P(\mathbf{q}) + i\eta} \right]. \quad (1)$$

In this expression \mathbf{k} and \mathbf{q} are Bloch wavevectors, m and n band indices, $\varepsilon_{n\mathbf{k}}$ and $\varepsilon_{m\mathbf{k}+\mathbf{q}}$ Kohn-Sham eigenvalues, $n_{\mathbf{q}}$ and $f_{m\mathbf{k}+\mathbf{q}}$ Bose-Einstein and Fermi-Dirac occupations, respectively, and η a positive infinitesimal. The summation runs over all states and the integral is over the Brillouin zone of volume Ω_{BZ} . The quantities $g_{mn}^{\text{eP}}(\mathbf{k}, \mathbf{q})$ represent the electron-plasmon scattering matrix elements between the initial state $\psi_{n\mathbf{k}}$ and the final state $\psi_{m\mathbf{k}+\mathbf{q}}$, and are given by:

$$g_{mn}^{\text{eP}}(\mathbf{k}, \mathbf{q}) = \left[\frac{\varepsilon_0 \Omega}{e^2 \hbar} \frac{\partial \epsilon(\mathbf{q}, \omega)}{\partial \omega} \right]_{\omega_P(\mathbf{q})}^{-\frac{1}{2}} \frac{1}{|\mathbf{q}|} \langle \psi_{m\mathbf{k}+\mathbf{q}} | e^{i\mathbf{q} \cdot \mathbf{r}} | \psi_{n\mathbf{k}} \rangle, \quad (2)$$

with Ω being the volume of one unit cell. Eqs. (1) and (2) are derived in the Supplemental Material [16]. The present approach to electron-plasmon coupling in semiconductors is formally identical to the standard theory of electron-phonon interactions [22]. In particular, the $1/|\mathbf{q}|$ divergence of the electron-plasmon matrix elements at long wavelengths is reminiscent of the Fröhlich interaction between electrons and longitudinal-optical phonons in polar semiconductors [23, 24]. This analogy is consistent with the fact that bulk plasmons are longitudinal waves. We now analyse the consequences of the self-energy in Eq. (1).

From the imaginary part of the self-energy in Eq. (1) we obtain the rate of electron scattering by thermal plasmons, using $\Gamma_{n\mathbf{k}} = 2 \text{Im } \Sigma_{n\mathbf{k}} / \hbar$. Physically the two denominators in Eq. (1) describe processes of one-plasmon absorption and emission, respectively. A diagrammatic representation of these processes is given in Fig. 2g. Multi-plasmon processes are not included in the present formalism, similarly to the case of electron-phonon interactions [22], therefore we limit our discussion to low temperatures ($n_{\mathbf{q}} \ll 1$). Fig. 2a shows the calculated electron-plasmon scattering rates in *n*-type silicon. The carrier energies are referred to the conduction band edge. For standard doping levels ($n < 10^{18} \text{ cm}^{-3}$) the scattering rates fall below 10^{11} s^{-1} as a result of the low inten-

sity of the plasmon peaks in Fig. 1e, which is reflected in the strength of the matrix elements in Eq. (2). However, at doping levels above 10^{18} cm^{-3} , the strength of the plasmon peak in the loss function increases considerably, and the frequency of scattering by thermal plasmons becomes comparable to electron-phonon scattering rates, 10^{12} - 10^{14} s^{-1} [25, 26]. Fig. 2a shows that at even higher doping levels these rates keep increasing by orders of magnitude, and eventually dominate the cooling dynamics of excited carriers.

A complementary perspective on the carrier dynamics is provided by Fig. 2b. Here we show the electron lifetimes corresponding to the rates in Fig. 2a, calculated as $\tau_{n\mathbf{k}} = 1/\Gamma_{n\mathbf{k}}$. Time-resolved reflectivity measurements of non-degenerate silicon ($n = 10^{17} \text{ cm}^{-3}$ electrons photo-excited at $\sim 0.8 \text{ eV}$ above the band edge) indicate thermalisation rates around 350 fs [27]. In the same doping range our calculations yield plasmon-limited carrier lifetimes well above 10 ps, indicating that under these conditions electron-plasmon scattering is ineffective. However, the scenario changes drastically for degenerate silicon, for which we calculate lifetimes in the sub-picosecond regime. In particular, for doping levels in the range 10^{19} - 10^{20} cm^{-3} the electron-plasmon scattering reduces the carrier lifetimes to 25-150 fs. In these conditions electron-phonon and electron-plasmon scattering become competing mechanisms for hot-carrier thermalisation.

In order to quantify the importance of electron-plasmon scattering we compare in Fig. 2c-e the imaginary part of the electron self-energy associated with (i) electron-plasmon interactions, (ii) electron-phonon interactions, and (iii) electron-hole pair generation. The methods of calculation of (ii) and (iii) are described in the Supplemental Materials [16]. From this comparison we deduce that plasmons become increasingly important towards higher doping, and their effect is most pronounced in the vicinity of the band edge. By identifying the largest contribution for each doping level and for each

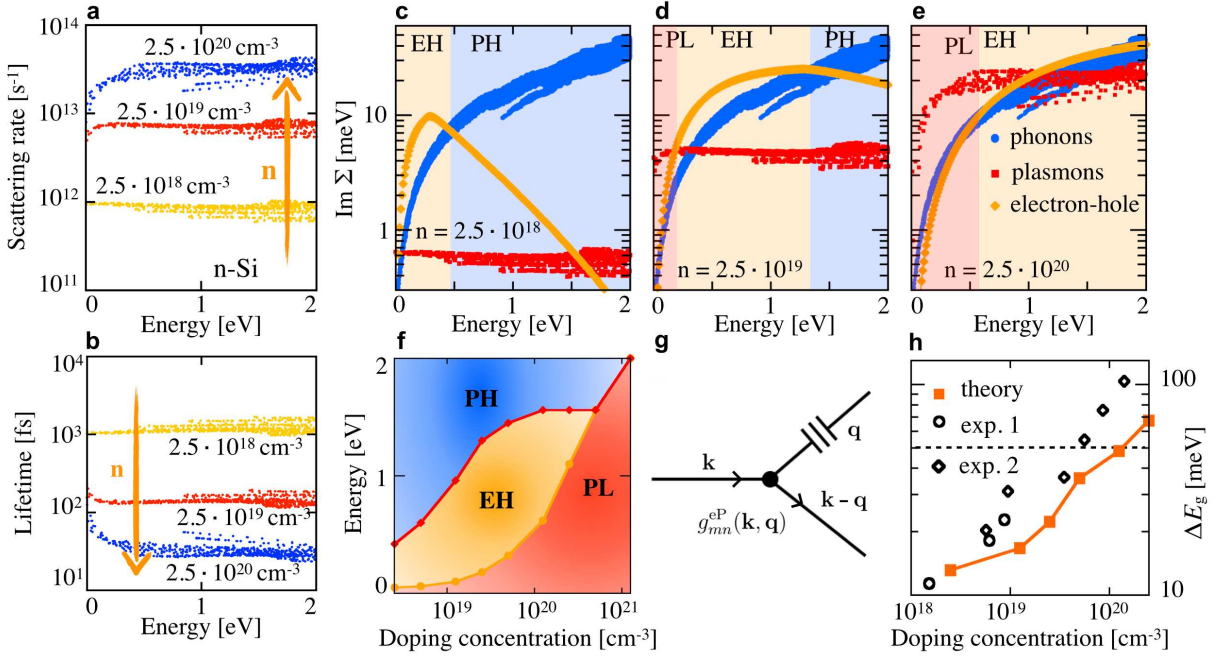


Figure 2. (a) Calculated rates of electron scattering by plasmons, and (b) corresponding electron lifetimes in doped silicon, for several carrier concentrations. The electron energy is referred to the conduction band edge. (c-e) Comparison between the imaginary part of the electron-plasmon self-energy, the electron-phonon self-energy, and the self-energy associated with electron-hole pair generation. The carrier concentration increases from (c) to (e), and the electron energy is referred to the conduction band edge. Shaded regions indicate the dominant scattering mechanism at a given electron energy, and ‘PL’, ‘PH’, ‘EH’ stand for plasmons, phonons, and electron-hole pairs, respectively. (f) Energy vs. doping map of the largest contribution to the electron self-energy. The energy is referred to the conduction band edge. (g) Diagrammatic representation of the electron plasmon scattering process. (h) Calculated plasmon-induced band gap renormalization in silicon as a function of carrier density (orange squares and line), compared to the optical data from Ref. [17] (experiment 1) and Ref. [18] (experiment 2). The dashed horizontal line indicates the renormalization of the band gap by electron-phonon interactions, as reported by Ref. [19].

electron energy, we can construct the ‘scattering phase diagram’ shown in Fig. 2f. This diagram illustrates the regions in the energy vs. doping space where each scattering mechanism dominates. Unexpectedly in degenerate silicon electron-plasmon scattering represents the dominant mechanism for hot-carrier relaxation. This finding could provide new opportunities in the study of semiconductor-based plasmonics, for example by engineering the doping concentration so as to selectively target the ‘plasmon region’ in Fig. 2f.

We also evaluated the impact of electron-plasmon scattering processes on the carrier mobility in silicon, by using the lifetimes computed above as a first approximation to the carrier relaxation times. As shown in Fig. S1 [16], the explicit inclusion of electron-phonon scattering is essential to achieve a good agreement with experiment. On the other hand, were we to consider only electron-phonon scattering and electron-hole pair generation, we would overestimate the experimental mobilities by more than an order of magnitude.

The real part of the electron self-energy in Eq. (1) allows us to evaluate the renormalization of the electron

energy levels arising from the dressing of electron quasi-particles by virtual plasmons. Since the renormalization of semiconductor band gaps induced by electron-phonon interactions attracted considerable interest lately [28–33], we here concentrate on the quantum zero-point renormalization of the fundamental gap of silicon. Computational details of the calculations and convergence tests are reported in the Supplemental Material [16]. Considering for definiteness a carrier density of $n = 2.5 \cdot 10^{20} \text{ cm}^{-3}$, we find that the electron-plasmon coupling lowers the conduction band edge by $\Delta E_c = -37 \text{ meV}$ at zero temperature, and rises the valence band edge by $\Delta E_v = 30 \text{ meV}$. For carrier concentrations of $2.5 \cdot 10^{19} \text{ cm}^{-3}$ and $2.5 \cdot 10^{20} \text{ cm}^{-3}$ we verified that the BGN changes by less than 1 meV for temperatures up to 600 K (see Supplemental Material [16]). As a result at this doping concentration the band gap redshifts by $\Delta E_g = \Delta E_c - \Delta E_v = -67 \text{ meV}$. This phenomenology is entirely analogous to the zero-point renormalization from electron-phonon interactions [29]. Our finding is consistent with the fact that the self-energy in Eq. (1) and the matrix element in Eq. (2) are formally identical to those that one encoun-

ters in the study of the Fröhlich interaction. The doping-induced band gap renormalization was also reported in a recent work on monolayer MoS₂ [34], therefore we expect this feature to hold general validity in doped semiconductors. In order to perform a quantitative comparison with experiment, we show in Fig. 2h our calculated plasmonic band gap renormalization and measurements of the indirect absorption onset in doped silicon [17, 18]. We can see that there is already good agreement between theory and experiment, even if we are considering only electron-plasmon couplings as the sole source of band gap renormalization. Surprisingly the magnitude of the renormalization, 15-70 meV, is comparable to the zero-point shift induced by electron-phonon interactions, 60-72 meV [19].

In summary, we presented an *ab initio* approach to electron-plasmon coupling in doped semiconductors. We showed that electron-plasmon interactions are strong and ubiquitous in a prototypical semiconductor such as doped silicon, as revealed by their effect on carrier dynamics, transport, and optical properties. This finding calls for a systematic investigation of electron-plasmon couplings in a wide class of materials. More generally, a detailed understanding of the interaction between electrons and thermal plasmons via predictive atomic-scale calculations could provide a key into the design of plasmonic semiconductors, for example by using phase diagrams such as in Fig. 2f to tailor doping levels and excitation energies to selectively target strong-coupling regimes. Finally, the striking similarity between electron-plasmon coupling and the Fröhlich coupling in polar materials may open new avenues to probe plasmon-induced photoemission kinks [35], polaron satellites [36–38], as well as superconductivity, in analogy with the case of electron-phonon interactions.[39–44].

F.C. acknowledges discussions with C. Verdi and S. Poncé. The research leading to these results has received funding from the Leverhulme Trust (Grant RL-2012-001), the Graphene Flagship (EU FP7 grant no. 604391), the UK Engineering and Physical Sciences Research Council (Grant No. EP/J009857/1). Supercomputing time was provided by the University of Oxford Advanced Research Computing facility (<http://dx.doi.org/10.5281/zenodo.22558>) and the ARCHER UK National Supercomputing Service.

-
- [1] S. Lal, S. Link, and N. J. Halas, *Nat. Photonics* **1**, 641 (2007).
 - [2] R. J. Walters, R. V. A. van Loon, I. Brunets, J. Schmitz, and A. Polman, *Nat. Mater.* **9**, 21 (2010).
 - [3] H. A. Atwater and A. Polman, *Nat. Mater.* **9**, 205 (2010).
 - [4] M. L. Brongersma, N. J. Halas, and P. Nordlander, *Nat. Nanotechnol.* **10**, 25 (2015).
 - [5] E. Y. Lukianova-Hleb, X. Ren, R. R. Sawant, X. Wu, V. P. Torchilin, and D. O. Lapotko, *Nat. Med.* **20**, 778 (2013).
 - [6] Z. Zhang, J. Wang, and C. Chen, *Adv. Mater.* **25**, 3869 (2013).
 - [7] S. Maier, *Plasmonics: Fundamentals and Applications* (Springer, 2007).
 - [8] J. M. Pitarke, V. M. Silkin, E. V. Chulkov, and P. M. Echenique, *Rep. Prog. Phys.* **70**, 1 (2007).
 - [9] E. Ozbay, *Science* **311**, 189 (2006).
 - [10] D. Bohm and D. Pines, *Phys. Rev.* **92**, 609 (1953).
 - [11] D. Pines and J. R. Schrieffer, *Phys. Rev.* **125**, 804 (1962).
 - [12] P. Nozières and D. Pines, *Phys. Rev.* **113**, 1254 (1959).
 - [13] S. L. Adler, *Phys. Rev.* **126**, 413 (1962).
 - [14] N. Wiser, *Phys. Rev.* **129**, 62 (1963).
 - [15] D. Pines, *Elementary Excitations in Solids* (Perseus, 1999).
 - [16] See Supplemental Material at [tobeaddedbypublisher](#), which includes Refs. [45–63].
 - [17] S. E. Aw, H. S. Tan, and C. K. Ong, *J. Phys.: Condens. Matter* **3**, 8213 (1991).
 - [18] M. Balkanski, A. Aziza, and E. Amzallag, *Phys. Status Solidi B* **31**, 323 (1969).
 - [19] M. Zacharias, C. E. Patrick, and F. Giustino, *Phys. Rev. Lett.* **115**, 177401 (2015).
 - [20] P. Nozieres and D. Pines, *Il Nuovo Cimento* (1955-1965) **9**, 470 (1958).
 - [21] G. Mahan, *Many-Particle Physics* (Springer, 2000).
 - [22] S. Engelsberg and J. R. Schrieffer, *Phys. Rev.* **131**, 993 (1963).
 - [23] H. Fröhlich, *Advances in Physics* **3**, 325 (1954).
 - [24] C. Verdi and F. Giustino, *Phys. Rev. Lett.* **115**, 176401 (2015).
 - [25] R. Jalabert and S. Das Sarma, *Phys. Rev. B* **41**, 3651 (1990).
 - [26] M. Bernardi, D. Vigil-Fowler, J. Lischner, J. B. Neaton, and S. G. Louie, *Phys. Rev. Lett.* **112**, 257402 (2014).
 - [27] F. E. Doany and D. Grischkowsky, *Appl. Phys. Lett.* **52** (1988).
 - [28] A. Marini, *Phys. Rev. Lett.* **101**, 106405 (2008).
 - [29] F. Giustino, S. G. Louie, and M. L. Cohen, *Phys. Rev. Lett.* **105**, 265501 (2010).
 - [30] E. Cannuccia and A. Marini, *Phys. Rev. Lett.* **107**, 255501 (2011).
 - [31] S. Botti and M. A. L. Marques, *Phys. Rev. Lett.* **110**, 226404 (2013).
 - [32] B. Monserrat, N. D. Drummond, C. J. Pickard, and R. J. Needs, *Phys. Rev. Lett.* **112**, 055504 (2014).
 - [33] G. Antonius, S. Poncé, P. Boulanger, M. Côté, and X. Gonze, *Phys. Rev. Lett.* **112**, 215501 (2014).
 - [34] Y. Liang and L. Yang, *Phys. Rev. Lett.* **114**, 063001 (2015).
 - [35] A. Damascelli, Z. Hussain, and Z.-X. Shen, *Rev. Mod. Phys.* **75**, 473 (2003).
 - [36] S. Moser, L. Moreschini, J. Jaćimović, O. S. Barišić, H. Berger, A. Magrez, Y. J. Chang, K. S. Kim, A. Bostwick, E. Rotenberg, L. Forró, and M. Grioni, *Phys. Rev. Lett.* **110**, 196403 (2013).
 - [37] F. Caruso, H. Lambert, and F. Giustino, *Phys. Rev. Lett.* **114**, 146404 (2015).
 - [38] F. Caruso and F. Giustino, *Phys. Rev. B* **92**, 045123 (2015).
 - [39] E. Bustarret, C. Marcenat, P. Achatz, J. Kacmarcik, F. Levy, A. Huxley, L. Ortega, E. Bourgeois, X. Blase, D. Debarre, and J. Boulmer, *Nature* **444**, 465 (2006).
 - [40] E. A. Ekimov, V. A. Sidorov, E. D. Bauer, N. N. Mel'nik,

- N. J. Curro, J. D. Thompson, and S. M. Stishov, *Nature* **428**, 542 (2004).
- [41] L. Boeri, J. Kortus, and O. K. Andersen, *Phys. Rev. Lett.* **93**, 237002 (2004).
- [42] K.-W. Lee and W. E. Pickett, *Phys. Rev. Lett.* **93**, 237003 (2004).
- [43] X. Blase, C. Adessi, and D. Connétable, *Phys. Rev. Lett.* **93**, 237004 (2004).
- [44] F. Giustino, M. L. Cohen, and S. G. Louie, *Phys. Rev. B* **76**, 165108 (2007).
- [45] L. Hedin, *Phys. Rev.* **139**, A796 (1965).
- [46] W. G. Aulbur, L. Jönsson, and J. W. Wilkins, *Solid State Phys.* **54**, 1 (2000).
- [47] M. S. Hybertsen and S. G. Louie, *Phys. Rev. B* **34**, 5390 (1986).
- [48] S. Engelsberg and P. M. Platzman, *Phys. Rev.* **148**, 103 (1966).
- [49] B. Lundqvist, *Phys. Kondens. Mater.* **6**, 193 (1967).
- [50] D. C. Langreth, *Phys. Rev. B* **1**, 471 (1970).
- [51] A. W. Overhauser, *Phys. Rev. B* **3**, 1888 (1971).
- [52] F. Mousty, P. Ostojia, and L. Passari, *J. Appl. Phys.* **45** (1974).
- [53] S. Das Sarma and F. Stern, *Phys. Rev. B* **32**, 8442 (1985).
- [54] J. R. Meyer and F. J. Bartoli, *Phys. Rev. B* **36**, 5989 (1987).
- [55] O. D. Restrepo, K. Varga, and S. T. Pantelides, *Appl. Phys. Lett.* **94**, 212103 (2009).
- [56] P. Hohenberg and W. Kohn, *Phys. Rev.* **136**, B864 (1964).
- [57] W. Kohn and L. J. Sham, *Phys. Rev.* **140**, A1133 (1965).
- [58] P. Giannozzi *et al.*, *J. Phys.: Condens. Matter* **21**, 395502 (2009).
- [59] N. Troullier and J. L. Martins, *Phys. Rev. B* **43**, 1993 (1991).
- [60] A. Marini, C. Hogan, M. Gruning, and D. Varsano, *Comp. Phys. Commun.* **180**, 1392 (2009).
- [61] J. Noffsinger, F. Giustino, B. D. Malone, C.-H. Park, S. G. Louie, and M. L. Cohen, *Comp. Phys. Commun.* **181**, 2140 (2010).
- [62] S. Baroni, S. de Gironcoli, A. Dal Corso, and P. Giannozzi, *Rev. Mod. Phys.* **73**, 515 (2001).
- [63] A. A. Mostofi, J. R. Yates, Y.-S. Lee, I. Souza, D. Vanderbilt, and N. Marzari, *Comp. Phys. Commun.* **178**, 685 (2008).